Consensus-Guided Correspondence Denoising

Chen Zhao[†*1], Yixiao Ge[†3], Jiaqi Yang[4], Feng Zhu[‡2], Rui Zhao[2], and Hongsheng Li[3]

[1]École Polytechnique Fédérale de Lausanne (EPFL)
[2]SenseTime Research
[3]CUHK-SenseTime Joint Lab, The Chinese University of Hong Kong
[4]School of Computer Science, Northwestern Polytechnical University

Abstract

Correspondence selection between two groups of feature points aims to correctly recognize the consistent matches (inliers) from the initial noisy matches. The selection is generally challenging since the initial matches are generally extremely unbalanced, where outliers can easily dominate. Moreover, random distributions of outliers lead to the limited robustness of previous works when applied to different scenarios. To address this issue, we propose to denoise correspondences with a local-to-global consensus learning framework to robustly identify correspondence. A novel "pruning" block is introduced to distill reliable candidates from initial matches according to their consensus scores estimated by dynamic graphs from local to global regions. The proposed correspondence denoising is progressively achieved by stacking multiple pruning blocks sequentially. Our method outperforms state-of-the-arts on robust line fitting, wide-baseline image matching and image localization benchmarks by noticeable margins and shows promising generalization capability on different distributions of initial matches.

1. Introduction

Accurate pixel-wise correspondences act as a premise to tackle many important tasks in computer vision and robotics, *e.g.*, Structure from Motion (SfM) [31], Simultaneous Location and Mapping (SLAM) [24], image stitching [5], visual localization [25], virtual reality [33], *etc*. But unfortunately, initial feature correspondences established by off-the-shelf detector-descriptors [20, 24, 22, 8] are far from satisfactory due to the possible challenging cross-image variations, *e.g.*, rotations, translations, scale changes, viewpoint changes, illumination changes, *etc*. Correspondence selection [40, 14] is therefore needed to select correct matches (inliers) and reject false matches (outliers), where deep learning-based methods [23, 39, 38, 32] have been proven effective.

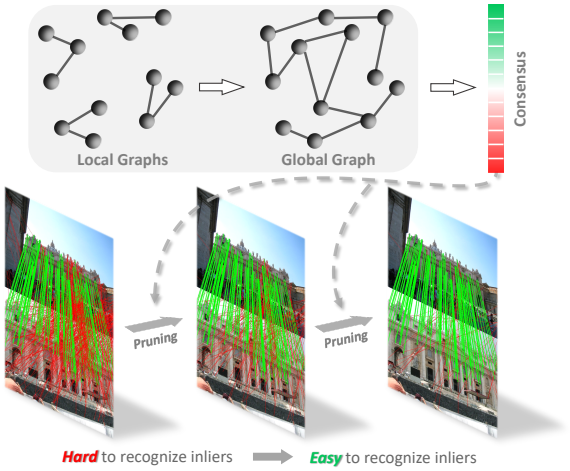

Figure 1. Correspondence denoising via local-to-global consensus learning. Given initial correspondences (bottom-left image) with dominant outliers, correctly recognizing inliers remains challenging. The correspondences are gradually tailored into reliable candidates (bottom-right image) based on their consensus scores estimated by local-to-global graphs, encouraging accurate inlier selection and robust model estimation.

Correspondence selection is generally cast as a per-match classification task in existing learning-based methods [23, 39, 38, 32], where Multi-Layer Perceptrons (MLPs) are adopted to classify putative matches into the subset of inliers or outliers. The optimization of such a binary classification problem is non-trivial, since the initial matches are likely to be extremely unbalanced with a ratio of around 90% for outliers [39]. Moreover, directly iden-

*The work was done when the author was an intern at SenseTime Research
†First two authors contributed equally
‡Corresponding author

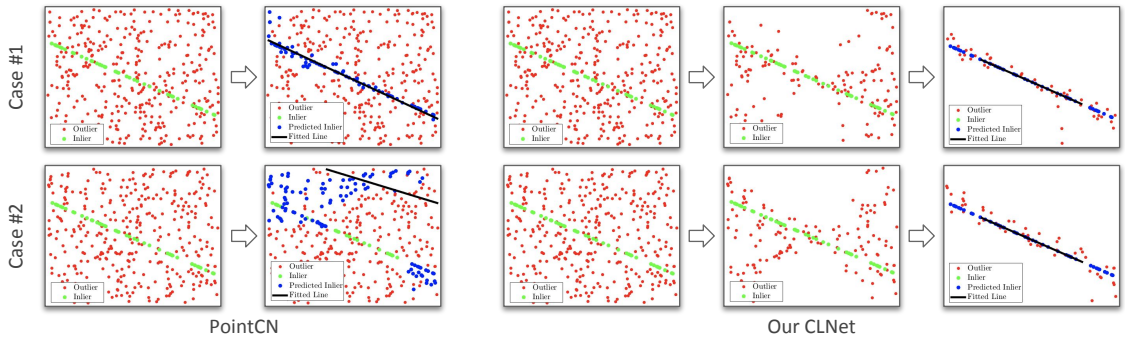

Figure 2. Robust line fitting under different distributions of outliers with PointCN [23] and our method, where inliers are identical in two cases while outliers are randomly sampled. PointCN fails in finding the correct solution in the second case, showing the inferior robustness under arbitrary outlier distributions. By contrast, our method gradually tailors the correspondences into reliable candidates for further line fitting, mitigating the effects of randomly sampled noises to large extent. The introduced denoising allows our method to be better generalized to different scenarios.

tifying inliers by two-class prediction is prone to suffering from randomly distributed outliers in real-world scenarios. We illustrate the above limitations in Fig. 2 via a toy line fitting task. It requires the model to fit a line from given data points corrupted by randomly sampled outliers. Note that we adopt identical inliers and different outliers in two cases. We observe that the baseline method PointCN [23] is not robust and fails in the second case.

Given the observed limitations of existing learning-based methods, we argue that properly *denoising* correspondences is crucial for robust model estimation, *i.e*. gradually tailor the noisy initial matches into reliable candidates (see Fig. 1). Such an intuition is inspired by the classic algorithm RANSAC [9], whose core idea is to sample the most reliable subset with sufficient inliers iteratively. The introduced correspondence denoising could largely mitigate the effects of unbalanced initial matches and stably improves the robustness of model estimation, since inliers are expected to account for a larger proportion in the selected subset than the one in raw matches. Apparently, a distinctive pruning is a cornerstone of the correspondence denoising. As one cannot classify given an isolated correspondence without context information, we propose to operate the pruning by a *local-to-global consensus learning* framework, which *explicitly* captures local and global context for correspondences.

Specifically, we *dynamically* construct local graphs for correspondences where the nodes (neighbors) and edges are determined from feature embeddings. An annular convolutional layer is introduced to estimate the consensus scores of aggregated features that represent the consistency in local graphs. The local graphs are further extended to a global graph guided by the local consensus scores, where the global consensus is described by a spectral graph convolutional layer [16]. The local and global consensus learning layers together form a novel "pruning" block, which preserves potential inliers with higher consensus scores while filters out noisy ones with lower scores. Our proposed correspondence denoising is progressively achieved by building up multiple pruning blocks sequentially. Such an architecture design encourages the refinement of local and global consensus learning at multiple scales. Note that the context information is *implicitly* modeled in previous works [23, 32] by feature normalization, while we *explicitly* exploit the context with local-to-global graphs. The superiority of our method is empirically shown in Sec. 4. Our contributions are summarized as three-fold.

- We for the first time propose to gradually prune correspondences for better inlier recognition and model estimation, which alleviates the effects of unbalanced initial matches and random outlier distributions.
- A local-to-global consensus learning framework is introduced to distill the putative correspondences into reliable candidates, where both local and global consensuses are properly estimated by establishing dynamic graphs on-the-fly*.
- We demonstrate the effectiveness of our method on the tasks of robust line fitting, wide-baseline image matching and image localization, where our method considerably outperforms state-of-the-art approaches.

2. Related Works

Generation-verification framework. The generation-verification framework has been widely used for robust model estimation, which iteratively generates hypotheses and verifies the hypothesis confidence, such as RANSAC [9], LO-RANSAC [7], PROSAC [6], USAC [27], NG-RANSAC [4], *etc*. Specifically, RANSAC [9] randomly samples a minimal subset of data points to estimate a parametric model, and then verifies its confidence

*The code will be released.

by evaluating the consistency between data points and the generated parametric model. NG-RANSAC [4] proposes a two-stage approach which improves the sampling strategy of RANSAC by a pre-trained deep neural network. RANSAC and its variations appear as powerful solutions when proper inliers exist in initial matches, where a reliable parametric model estimated from a noise-free sampling can be expected after iterations. But unfortunately, such kind of pipeline is vulnerable to enormous outliers due to the inevitable noise in sampled subsets.

Per-match classification. Inspired by the tremendous success of deep learning [12, 28, 17], it is desirable to perform correspondence selection via deep networks. However, it is non-trivial to employ 2D convolutions to consume correspondences due to the irregular and unordered characteristics. As a pioneer in learning-based methods, PointCN [23] treats the correspondence selection as a per-match classification, using MLPs to predict the label (inlier or outlier) for each correspondence. Following PointCN, the per-match classification becomes a mainstream. NM-Net [39] expects to extract reliable local information for correspondences via a compatibility-specific mining, which relies on the known affine attributes. OANet [38] presents a combination of differentiable pooling and unpooling to describe local context and generate the full size prediction, respectively. An attentive context normalization is proposed in [32], which implicitly represents global context by the weighted mean and variance. Although existing methods have shown satisfactory performance, they still suffer from the issue of dominant outliers in the putative correspondences. To address this issue, we suggest denoising correspondences into reliable candidates for more robust model estimation. Correspondence denoising is found effective to mitigate the effects of noisy outliers to large extent (Please see Sec. 4).

Consensus in correspondences. Correct matches have been proven consistent in epipolar geometry or under the homography constraint [11], while mismatches are inconsistent because of the random distribution. The consensus in correspondences has been studied by hand-crafted methods in the literature. GTM [1] performs game-theoretic matching based on a payoff function which utilizes affine information around keypoints to measure the consistency between a pair of correspondences. LPM [21] assumes that local geometry around correct matches does not change freely. The geometry variation is represented by the consensus of k-nearest neighbors on keypoint coordinates, which is not discriminative enough as evaluated in [40]. Inspired by the hand-crafted efforts, we suggest *learning* consensus via local-to-global graphs.

3. Method

To tackle the challenge of noisy initial correspondences, we present a local-to-global **C**onsensus **L**earning framework (**CLNet**) (see Fig. 3), which consists of sequential "pruning" blocks. The key innovation of our framework lies in progressively tailoring the putative correspondences into more reliable candidates by exploiting their consensus scores, which are learned from dynamic local-to-global graphs. A parametric model is estimated from the most confident inliers in the denoised subset and further employed to determine inliers and outliers out of full-size putative correspondences. In order to encourage a continuous latent space for more accurate consensus estimation, we introduce to use adaptive temperatures in the inlier/outlier classification losses as the training objective.

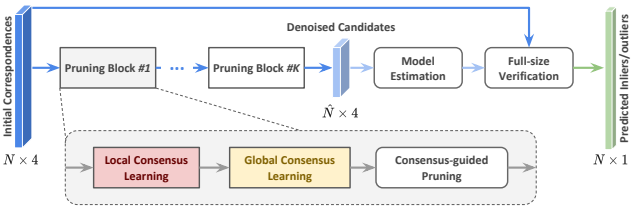

Figure 3. Overall framework. N represents the number of matches and 4 denotes 4D locations of matched keypoints. Raw data are gradually tailored into $\hat{N}$ candidates with K pruning blocks guided by local-to-global consensus learning. A parametric model is estimated from $\hat{N}$ denoised candidates and is further employed for the full-size verification, yielding $N \times 1$ inlier/outlier predictions for initial correspondences.

3.1. Problem Formulation

Given an image pair $(\mathbf{I}, \mathbf{I}')$, putative correspondences $\boldsymbol{C}$ can be established via nearest neighbor matching between extracted keypoints according to the corresponding descriptors, denoted as $\boldsymbol{C} = [\boldsymbol{c}_1, \cdots, \boldsymbol{c}_N] \in \mathbb{R}^{N\times 4}$. $\boldsymbol{c}_i = [x_i, y_i, x_i', y_i']$ indicates a correspondence between a keypoint (x_i, y_i) in the image $\mathbf{I}$ and another keypoint (x_i', y_i') in the paired image $\mathbf{I}'$. There is no restriction on the off-the-shelf detectors or descriptors, either handcrafted methods [20, 29] or learned ones [22, 8] are compatible. As the putative correspondences $\boldsymbol{C}$ are prone to containing enormous mismatches, the task of correspondence selection is introduced to select the correct matches (inliers) $\boldsymbol{C}_p$ and reject the noisy ones (outliers) $\boldsymbol{C}_n$.

Existing learning-based methods [23, 32] generally cast the correspondence selection task as an inlier/outlier classification problem by adopting permutation-invariant neural networks to predict inlier weights $\boldsymbol{w} = \tanh(\mathrm{ReLU}(\boldsymbol{o})) \in [0, 1)$ for all putative correspondences $\boldsymbol{C}$, where $\boldsymbol{o}$ is the output of networks. It is worth noting that only $\boldsymbol{C}$ serves as input for the networks. The correspondence $\boldsymbol{c}_i \in \boldsymbol{C}$ will be categorized into outliers $\boldsymbol{C}_n$ if its predicted weight $w_i = 0$. The predicted weights $\boldsymbol{w}$ are not only utilized to recognize inliers but also employed as an auxiliary input for model estimation, *e.g.* yielding the essential matrix $\hat{\boldsymbol{E}}$ for camera pose estimation [11].

3.2. Local-to-Global Consensus Learning

Predicting accurate weights $\boldsymbol{w}$ is at the core of learning-based correspondence selection methods. However, it is non-trivial due to the dominant outliers in putative correspondences. Specifically, the initial matches are prone to being extremely unbalanced with over 90% outliers [39] for each image pair. The outliers are randomly distributed in real-world scenarios which might not be "seen" from the training samples. We argue that existing methods [23] heavily suffer from this issue since training a network to perform full-size per-match classification straightforwardly is sub-optimal.

Correspondence denoising. By contrast, we introduce to gradually tailor the putative correspondences $\boldsymbol{C}$ into reliable candidates $\hat{\boldsymbol{C}}$ by removing most outliers, mitigating the effects of randomly distributed outliers to large extent. By predicting inlier weights $\hat{\boldsymbol{w}}$ for the denoised subset $\hat{\boldsymbol{C}}$, we can expect more confident inliers $\hat{\boldsymbol{C}}_p$ and regress a more accurate parametric model (essential matrix $\hat{\boldsymbol{E}}$ as an example) from $\hat{\boldsymbol{C}}_p$. In turn, the computed model can be adopted to perform a full-size verification on the entire set $\boldsymbol{C}$ for specific applications, *e.g.* image localization. Our solution, therefore, becomes a "generation-verification" pipeline, which is inspired by classic and effective algorithm RANSAC [9], such that

$$\begin{aligned}(\hat{\boldsymbol{w}}, \hat{\boldsymbol{C}}) &= f_\phi(\boldsymbol{C}),\\ \hat{\boldsymbol{E}} = g(\hat{\boldsymbol{w}}, \hat{\boldsymbol{C}}), &\quad \boldsymbol{w} = h(\hat{\boldsymbol{E}}, \boldsymbol{C}),\end{aligned} \tag{1}$$

where f_ϕ is a deep neural network with learnable parameters ϕ that performs correspondence denoising and weight predicting simultaneously. $g(\cdot,\cdot)$ denotes parametric model estimation (generation) and the optional $h(\cdot,\cdot)$ performs full-size predictions (verification).

As inliers in $\boldsymbol{C}_p$ are expected to be consistent in both local and global contexts, we propose to estimate local-to-global consensus scores for correspondences. Correspondences with higher scores are preserved and the remaining is immediately removed as outliers. Note that the consensus scores also serve as inlier weights in our work, so we use a unified notation $\boldsymbol{w}$ for these two concepts. The local and global consensus layers are used sequentially, forming a novel pruning module, dubbed "pruning" block in our paper. As illustrated in Fig. 3, multiple "pruning" blocks are established for progressive denoising, *i.e.* $\boldsymbol{C} \rightarrow \cdots \rightarrow \hat{\boldsymbol{C}}$. The detailed network architecture of each "pruning" block can be found in Fig. 4. Without loss of generality, we assume that the input for a "pruning" block is $\boldsymbol{C} \in \mathbb{R}^{N\times 4}$ and the output is $\hat{\boldsymbol{C}} \in \mathbb{R}^{\hat{N}\times 4}$ in the remainder of this section, where $\hat{N} < N$.

Local consensus. We propose to leverage local context for each anchor correspondence $\boldsymbol{c}_i$, building upon a graph with its k-nearest neighbors, denoted as

$$\mathcal{G}_i^l = (\mathcal{V}_i^l, \mathcal{E}_i^l), \quad 1 \le i \le N, \tag{2}$$

where $\mathcal{V}_i^l = \{\boldsymbol{c}_i^1, \cdots, \boldsymbol{c}_i^k\}$ is the set of k-nearest neighbors for $\boldsymbol{c}_i$, and $\mathcal{E}_i^l = \{\boldsymbol{e}_{i1}^l, \cdots, \boldsymbol{e}_{ik}^l\}$ indicates edges describing the affinities between $\boldsymbol{c}_i$ and its neighbors in $\mathcal{V}_i^l$.

Specifically, given an input correspondence $\boldsymbol{c}_i \in \boldsymbol{C}$, we encode it into a feature representation $\boldsymbol{z}_i$ by a series of ResNet blocks [12]. The k-nearest neighbors for each $\boldsymbol{c}_i$ are determined by ranking the Euclidean distances between $\boldsymbol{z}_i$ and other features $\{\boldsymbol{z}_j | 1 \le j \le N, j \ne i\}$. Following [36], we utilize the concatenated anchor feature and residual feature as the edge, denoted as

$$\boldsymbol{e}_{ij}^l = [\boldsymbol{z}_i, \boldsymbol{z}_i - \boldsymbol{z}_i^j], \quad 1 \le j \le k \tag{3}$$

where $\boldsymbol{z}_i^j$ is the feature representation of $\boldsymbol{c}_i$'s j-th neighbor and $\boldsymbol{e}_{ij}^l$ is the edge linking $\boldsymbol{c}_i$ and $\boldsymbol{c}_i^j$ in the local graph.

Given the established local graphs, our goal is to describe the local consensus represented by a consensus score for each anchor correspondence. Intuitively, we can split such a process into two steps: 1) aggregating the feature $\boldsymbol{z}_i \rightarrow \tilde{\boldsymbol{z}}_i$ by passing messages along graph edges $\mathcal{E}_i^l$, and 2) predicting a consensus score for $\tilde{\boldsymbol{z}}_i$ via MLPs. A naïve way for feature aggregation is using convolutions followed by pooling layers [36] (will be discussed in Table 4). However, this operation may lose the structural information in the graphs, *i.e.* the k-nearest neighbors in $\mathcal{V}_i^l$ are actually sorted by their affinities and should be treated differently. To make the most of the graph knowledge, we propose a novel *annular* convolutional layer (shown in Fig. 5), gradually aggregating features in groups. In detail, we assign the nodes in $\mathcal{V}_i^l$ into k/p annuli, where p denotes the number of nodes in each annulus and k is expected to be divisible by p. We aggregate the features in each annulus via a convolution kernel as

$$\text{out} = \mathbf{W}^l \mathcal{E}_i^l(s) + \mathbf{b}^l, \quad 1 \le s \le \frac{k}{p}, \tag{4}$$

where $\mathcal{E}_i^l(s)$ is a subset of $\mathcal{E}_i^l$, $\mathbf{W}^l$ and $\mathbf{b}^l$ are learned weights and bias for the convolution. k/p aggregated features are further integrated by another annular convolution (see the second one in Fig. 5), where the parameters $\mathbf{W}^l$ and $\mathbf{b}^l$ do not share among different annular convolutional layers.

Subsequently, several ResNet blocks are adopted for feature embedding, yielding $\tilde{\boldsymbol{z}}_i$. We further encode the aggregated feature $\tilde{\boldsymbol{z}}_i$ into a local consensus score w_i^l which reflects the consistency of $\boldsymbol{c}_i$ in the local receptive field. In other words, w_i^l roughly measures the inlier weights of $\boldsymbol{c}_i$ when only considering the local context.

Global consensus. As aforementioned, the local consensus scores $\{w_1^l, \cdots, w_N^l\}$ evaluate the correspondence consistency in the fractional context, which only consider a limited k-nearest region. To this end, we introduce to estimate

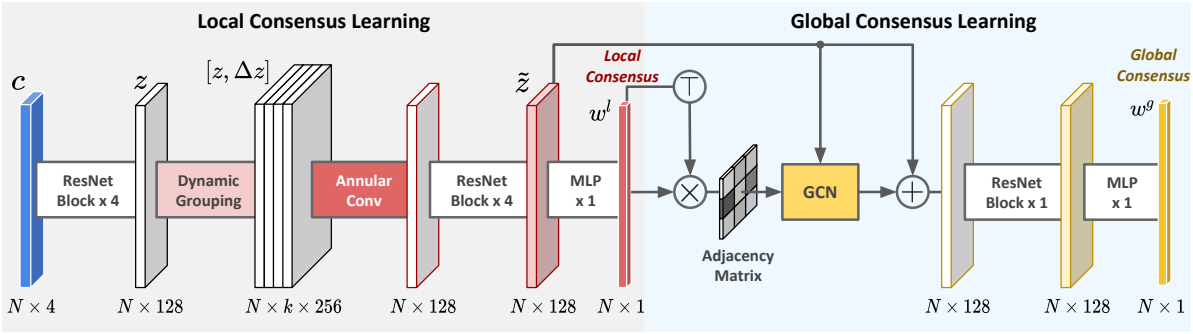

Figure 4. Detailed architecture of the proposed pruning block, which consists of local-to-global consensus learning layers. Each ResNet block [12] contains two MLPs followed by Context Normalization [23], Batch Normalization [13], and ReLU. Note that Attentive Context Normalization [32] is not used in our method, because it requires additional supervisions. According to the estimated global consensus scores, the reliable candidates of input correspondences can be selected.

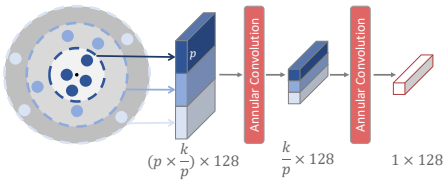

Figure 5. Illustration of the proposed annular convolution. The nodes (colored dots) in a local graph are assigned into annuli based on affinities to the anchor. The features in each annulus are aggregated by a convolution kernel.

full-size correlations via connecting local graphs to a global one. We denote the global graph as

$$\mathcal{G}^g = (\mathcal{V}^g, \mathcal{E}^g), \tag{5}$$

where the nodes $\mathcal{V}^g$ are represented by local aggregated features $\{\tilde{\boldsymbol{z}}_1, \cdots, \tilde{\boldsymbol{z}}_N\}$. The edges $\mathcal{E}^g$ that indicate the compatibility of pairs of correspondences, are estimated based on local consensus scores $\boldsymbol{w}^l$. Specifically, an edge $\boldsymbol{e}^g_{ij} \in \mathcal{E}^g$ is computed by

$$\boldsymbol{e}^g_{ij} = w^l_i \cdot w^l_j, 1 \leq i, j \leq N. \tag{6}$$

Using all the entries in $\mathcal{E}^g$, the adjacency matrix $\mathbf{A} \in \mathbb{R}^{N \times N}$ ($\mathbf{A}_{ij} = \boldsymbol{e}^g_{ij}$) is formed which explicitly describes global context. Subsequently, the graph Laplacian for the GCN layer [16] is approximated as

$$\mathbf{L} = \widetilde{\mathbf{D}}^{-\frac{1}{2}} \widetilde{\mathbf{A}} \widetilde{\mathbf{D}}^{-\frac{1}{2}}, \tag{7}$$

where $\widetilde{\mathbf{A}} = \mathbf{A} + \mathbf{I}_N$ for numerical stability, and $\widetilde{\mathbf{D}} \in \mathbb{R}^{N \times N}$ is the diagonal degree matrix of $\widetilde{\mathbf{A}}$. The global embedding is then acquired by

$$\text{out} = \mathbf{L} \cdot [\tilde{\boldsymbol{z}}_1, \cdots, \tilde{\boldsymbol{z}}_N] \cdot \mathbf{W}^g, \tag{8}$$

where $\{\tilde{\boldsymbol{z}}\}$ are aggregated features yield by the local consensus learning and $\mathbf{W}^g$ is a learnable matrix. $\mathbf{L}$ modulates $\{\tilde{\boldsymbol{z}}\}$ into the spectral domain, considering the isolated local embeddings in a joint manner. The feature filters in the spectral domain enable the propagated features to be capable of reflecting the consensus from the global graph Laplacian. Similar to the local consensus learning, global consensus scores $\boldsymbol{w}^g$ are estimated by encoding the aggregated features via a ResNet block followed by MLPs.

Consensus-guided pruning. Since the global consensus scores jointly consider both global and local context, we prune the putative correspondences based on their global consensus scores $\boldsymbol{w}^g$. Specifically, elements in $\boldsymbol{C}$ are sorted in a descending order by $\boldsymbol{w}^g$. The top-$\hat{N}$ correspondences are preserved and the remaining ones are removed as noisy outliers. Besides, inspired by [38], we employ an iterative design, which takes local and global consensus scores as additional input to the next pruning block. A ResNet block and MLPs are used after the last pruning block to predict inlier weights $\hat{\boldsymbol{w}}$ of the denoised candidates for the weighted model estimation.

Training objectives. Learning-based correspondence selection methods [23, 32] generally require an inlier/outlier classification loss and an regression loss for model estimation as the training objective. For camera pose estimation, the ground-truth labels *vs*. of $\boldsymbol{C}$ are assigned by epipolar distances with an ad-hoc threshold d_{thr} on widely-used benchmarks [38, 14], which is empirically set as $1e$-4.

Although training with a conventional binary cross-entropy loss has achieved satisfactory performance, we argue that inevitable label ambiguity exists, especially for the correspondences whose epipolar distances are around d_{thr}. Intuitively, the confidence of $\boldsymbol{c}_i$ should be negatively correlated to the corresponding epipolar distance d_i, *i.e.* $d_i \to 0$ for an inlier. To this end, we introduce an adaptive temperature for putative inliers ($d_i < d_{\text{thr}}$), which is computed by a Gaussian kernel

$$\tau_i = \exp(-\frac{\|d_i - d_{\text{thr}}\|_1}{\alpha \cdot d_{\text{thr}}}), \tag{9}$$

where α is the kernel width. For outliers $\boldsymbol{c}_i$ with $d_i >= d_{\text{thr}}$,

we set $\tau_i = 1$. Note that the error of label assignment cannot be eliminated due to the inherent ambiguity of epipolar constraint [11]. The overall training objective is denoted as

$$\mathcal{L} = \mathcal{L}_{\text{cls}} + \lambda \mathcal{L}_{\text{reg}}(\hat{\mathbf{E}}, \mathbf{E}), \tag{10}$$

where $\mathcal{L}_{\text{reg}}$ represents a regression loss [38] on estimated parametric model $\hat{\mathbf{E}}$, and λ is a weighting factor. The binary classification loss $\mathcal{L}_{\text{cls}}$ with our proposed adaptive temperature is formulated as

$$\begin{aligned}\mathcal{L}_{\text{cls}} = \sum_{j=1}^{K} \Big(& \ell_{\text{bce}}(H(\mathbf{o}_j^l), \mathbf{y}_j) + \ell_{\text{bce}}(H(\mathbf{o}_j^g), \mathbf{y}_j) \Big) \\ & + \ell_{\text{bce}}(H(\hat{\mathbf{o}}_j), \hat{\mathbf{y}}_j),\end{aligned} \tag{11}$$

where $\boldsymbol{o}_j^l$, $\boldsymbol{o}_j^g$ are the outputs of local and global consensus learning layers in j-th pruning block, respectively, $\hat{\mathbf{o}}_j$ is the output of the last MLP in CLNet (recall that $\boldsymbol{w} = \tanh(\text{ReLU}(\boldsymbol{o}))$); $H(\mathbf{o}) = \sigma(\boldsymbol{\tau} \cdot \mathbf{o})$ (σ is the sigmoid activation); $\mathbf{y}_j$, $\hat{\mathbf{y}}_j$ denote the set of binary ground-truth labels; ℓ_{bce} indicates a binary cross-entropy loss; K is the number of pruning blocks. As a result, an inlier c_i with a smaller d_i would be more confident to enforce larger regularization on the model optimization via a smaller temperature.

4. Experiments

Experiments are conducted on four datasets, covering the tasks of robust line fitting (Sec. 4.2), wide-baseline image matching (Sec. 4.3), and image localization (Sec. 4.4). Comprehensive analyses in Sec. 4.5 demonstrate the effectiveness of each component in our method.

4.1. Implementation Details

Two pruning blocks are adopted sequentially, tailoring the putative N correspondences into $N/4$ candidates, *i.e.* pruning by half for each block. We set $k = 9$ and $k = 6$ as the number of nearest neighbors in two blocks when establishing local graphs, respectively. We use $p = 3$ in Eq. (4), $\alpha = 1$ in Eq. (9), and $\lambda = 0.5$ in Eq. (10). ADAM optimizer is employed with a batch size of 32 and constant learning rate of 10^{-3} for training.

4.2. Robust Line Fitting

Let us assume a 2D line as $ax + by + c = 0$ with randomly sampled parameters (a, b, c) from $[0, 1]$. Inliers are generated by randomly sampling $x \in [-5, 5]$ and then estimating y by the equation. Outliers are taken into account via randomly locating (x, y) in $[-5, 5]$. 1000 points $(N = 1000)$ are selected in total to fit each line by determining inliers from noisy data and approximating (a, b, c) by Least Squares [18]. We use $6,000$ and $2,000$ samples for training and testing, respectively.

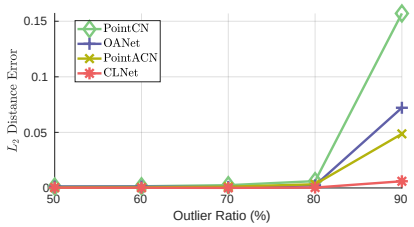

Figure 6. Line fitting performance. The methods are tested on five datasets where the outlier ratio varies from 50% to 90%. The evaluation metric is L_2 distance between the predicted line parameters and the ground-truth ones.

The results of line fitting are illustrated in Fig. 6. PointCN [23], OANet [38], and PointACN [32] are retrained on the synthetic data, using official codes released by the authors. We add different levels of perturbations by varying the outlier ratio from 50% to 90%. The L_2 distance between ground-truth (a, b, c) and predicted ones is reported. Compared with competitors, our method generalizes well in all five levels and achieves significantly superior results in the hardest case, *i.e.* 90% outliers.

4.3. Wide-baseline Image Matching

We conduct experiments of wide-baseline image matching for camera pose estimation. The experiments are performed on the outdoor YFCC100M [34] and indoor SUN3D [37] datasets, following the settings in [38]. As suggested in [23, 38, 32], a weighted 8-point algorithm is used in our model estimation to compute the essential matrix ($\hat{\boldsymbol{E}}$) with denoised candidates $\hat{\boldsymbol{C}}$, which is pivotal to recover camera poses. Keypoint coordinates in $\boldsymbol{C}$ are normalized using camera intrinsics [23]. Epipolar distances of $\boldsymbol{C}$ are estimated under the constraint of $\hat{\mathbf{E}}$ and then compared with a threshold ($d_{\text{thr}} = 1e\text{-}4$ by default) to perform a full-size verification. The mean average precision (mAP) of recovered poses under different error thresholds is reported. We also evaluate the inlier/outlier classification results by precision, recall, and F-measure [39].

Table 1 lists the quantitative results on YFCC100M and SUN3D. For hand-crafted methods, *i.e.* RANSAC [9] and MAGSAC [3], we clean the initial correspondences by ratio test [20] with a threshold of 0.8, because the results without ratio test are significantly worse than other competitors. For learned methods, the initial correspondences are immediately consumed. The solution that uses RANSAC as a post-processing of learned approaches is also considered. Note that SuperGlue [30] is not compared since it targets at another task, *i.e.* predicting high-quality *initial* matches rather than correspondence selection. As reported, CLNet delivers the best mAP5 and F-measure on both two datasets. It achieves 53.15% mAP5 and 79.72% F-measure on YFCC100M, which outperforms other approaches by noticeable margins, *i.e.* over 10%. The ground-truth la-

	YFCC100M [34] (outdoor) (%)						
	mAP5	mAP10	mAP15	mAP20	Precision	Recall	F-measure
RANSAC [9]	30.25/-	39.58/-	46.02/-	50.64/-	74.92	51.98	60.35
MAGSAC [3]	32.80/-	41.61/-	47.70/-	52.20/-	73.00	14.42	23.56
PointCN [23]	49.75/29.80	59.66/42.65	65.94/51.33	70.07/57.74	55.80	84.32	64.51
NM-Net [39]	51.90/32.93	61.75/46.85	67.99/55.98	72.27/62.51	55.30	85.80	64.71
OANet [38]	51.98/35.30	61.76/48.49	67.98/57.38	72.13/63.43	55.35	83.37	64.79
OANet++ [38]	52.48/40.93	62.74/54.56	68.87/62.70	72.82/67.93	53.80	87.57	63.99
PointACN [32]	52.56/42.80	62.05/56.76	68.60/64.99	72.70/70.42	53.85	**88.56**	64.01
Our CLNet	**58.70/53.15**	**68.86/64.85**	**74.85/71.77**	**78.72/76.19**	**85.20**	76.04	**79.72**

	SUN3D [37] (indoor) (%)						
	mAP5	mAP10	mAP15	mAP20	Precision	Recall	F-measure
RANSAC [9]	9.97/-	16.24/-	21.70/-	26.21/-	59.81	29.98	38.00
MAGSAC [3]	13.15/-	20.35/-	26.02/-	30.60/-	56.89	0.08	13.17
PointCN [23]	15.55/9.82	24.51/18.44	31.33/25.96	36.72/32.09	47.28	82.85	56.48
NM-Net [39]	16.86/14.13	25.55/24.01	32.56/31.85	38.09/38.19	46.68	83.98	56.34
OANet [38]	17.41/15.56	27.22/26.19	34.33/34.37	40.00/40.76	47.21	84.04	56.73
OANet++ [38]	17.29/16.85	26.69/27.20	33.80/35.30	39.36/41.65	47.12	84.21	56.81
PointACN [32]	17.09/17.44	26.67/28.23	34.01/**36.62**	39.78/**43.24**	46.62	**85.30**	56.25
Our CLNet	**19.12/17.86**	**29.42/28.35**	**37.07**/36.29	**42.91**/42.52	**68.93**	66.59	**65.13**

Table 1. Performance on YFCC100M [34] and SUN3D [37], in terms of mAP on recovered poses, precision, recall and F-measure metrics on inlier recognition. As for the mAP, **-/-** represents results **with/without** RANSAC post-processing. Ratio test is employed as a pre-processing technique for both RANSAC and MAGSAC.

	SUN3D [37] (%)	YFCC100M [34] (%)	
	SIFT [20]	ORB [29]	DoG-HardNet [22]
PointCN [23]	1.39	9.65	29.45
NM-Net [39]	0.94	10.45	29.65
OANet++ [38]	2.91	13.00	41.88
PointACN [38]	1.83	12.38	41.70
Our CLNet	**3.73**	**14.70**	**49.68**

Table 2. Evaluation on the generalization capability. All the models are trained on YFCC100M [34] with SIFT [20], and are directly tested on SUN3D [37] with SIFT and YFCC100M with ORB [29] and DoG-HardNet [22]. mAP5 (%) is reported.

bel assignments of SUN3D dataset are considerably ambiguous due to the repeatable and low texture [23], making RANSAC an important role for data post-processing [14]. Our CLNet-RANSAC combination outperforms all state-of-the-arts and CLNet alone achieves competitive performance on SUN3D. Note that previous learning-based methods, *e.g.* PointACN as well as OANet++, cannot be well compatible with RANSAC, showing inferior final performance, which would limit their applications in real-world scenarios.

We take the generalization capacity into account by testing learned methods on SUN3D with SIFT and YFCC100M with ORB [29] and DoG-HardNet [22]. We choose ORB and DoG-HardNet to generate initial matches with two different data distributions, because the former one has been widely used in SLAM [24] and the latter one is the most robust detector-descriptor combination evaluated in [14]. The tested models are trained on YFCC100M with SIFT. As listed in Table 2, CLNet achieves the best performance under all settings, which shows the flexibility of our method on different datasets and detector-descriptor combinations.

4.4. Image Localization

We consider an application of image-based localization, which aims at localizing a query image by retrieving nearby reference images with geographical tags [10]. Existing image-based methods [2, 10] take raw images as input and learn discriminative feature descriptors for retrieval. We suggest utilizing correspondence-based methods as a post-processing technique of image-based ones to achieve a coarse-to-fine localization, where three steps are adopted. 1) Image-based methods [2, 10] are used to search for top-k (k is empirically set as 100) images for each query. We did not use all reference images for re-ranking due to the intractable time consuming. 2) Feature matching techniques [20, 9, 23] are then carried out on each pair of the retrieved reference image and the query image, achieving putative correspondences. 3) The top-k images are re-ranked by the refined similarity. Specifically, the similarity between each query image and gallery image is refined by $S_{\text{img}} + S_{\text{inl}}$, where S_{img} represents the original similarity estimated by image-based methods, and S_{inl} is the normalized inlier number within $[0, 1]$.

In the experiments, we use state-of-the-art SFRS [10] as the image-based method and employ correspondence-based RANSAC [9], PointCN [23] and our CLNet as the post-processing technique. Note that PointCN and CLNet

Method	Tokyo 24/7 [35] (%)		
	R@1	R@5	R@10
NetVLAD [2]	73.3	82.9	86.0
CRN [15]	75.2	83.8	87.3
SARE [19]	79.7	86.7	90.5
SFRS [10]	85.4	91.1	93.3
RANSAC [9]-SFRS	88.6 (+3.2)	93.0 (+1.9)	93.7 (+0.4)
PointCN [23]-SFRS	89.5 (+4.1)	93.3 (+2.2)	94.3 (+1.0)
Our CLNet-SFRS	**91.4 (+6.0)**	**94.0 (+2.9)**	**94.3 (+1.0)**

Table 3. Evaluation on the image localization dataset Tokyo 24/7 [35], in terms of Recall@1/5/10.

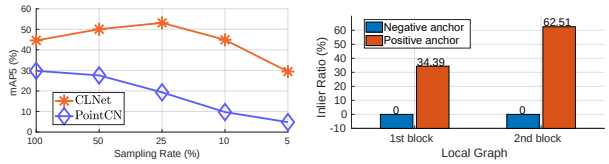

(a) (b)

Figure 7. (a) shows mAP5 of poses estimated from candidates sampled by CLNet and PointCN [23] under different sampling ratios; (b) illustrates inlier ratios of nodes in local graphs anchored by inliers (positive anchor) and outliers (negative anchor) in CLNet.

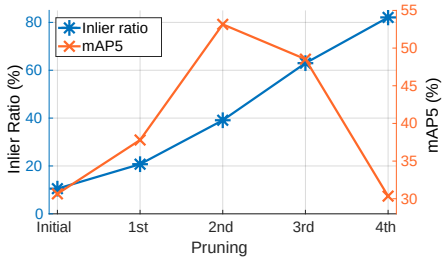

Figure 8. The inlier ratio of candidates (blue line) and mAP5 of poses (orange line) estimated by CLNet with different pruning iterations.

are pretrained on YFCC100M [34]. As shown in Table. 3, CLNet further improves SFRS with noticeable 6.0% gains in terms of Recall@1. Since image-based methods focus on global descriptors, while correspondence-based methods pay more attention on local patterns, these two kinds of methods can be well compatible with each other. The superiority of our method can also be observed by comparing "CLNet-SFRS" with "RANSAC-SFRS" and "PointCN-SFRS", where our CLNet achieves more advanced performance than both RANSAC and PointCN.

4.5. Ablation Studies

Consensus-guided pruning. To distill candidates from initial data, a vanilla solution is to sample matches according to the weights predicted by off-the-shelf methods, *e.g.* PointCN [23]. One may consider if consensus learning is an over-kill for pruning. To address this issue, we use PointCN to replace consensus learning for pruning as a fair comparison. Specifically, PointCN pretrained on YFCC100M is iteratively performed twice in the inference phase. Initial matches are tailored into a specific number of candidates in the first iteration, and the pruned correspondences are consumed to estimate essential matrices in the second iteration. Fig. 7(a) shows the results with different sampling rates on YFCC100M. We observe that the mAP5 of PointCN declines as the sampling rate gets smaller. It suggests that it is non-trivial to carry out an effective pruning for camera pose estimation. By contrast, Our method significantly outperforms PointCN-guided pruning, achieving the optimal mAP5 with a sampling rate of 25%. The effectiveness of our consensus learning is further explained in Fig. 7(b), which illustrates the inlier ratios of nodes in local graphs. The grouped neighbors are significantly more consistent with higher inlier ratios when graphs are anchored by inliers. The results demonstrate that our method is well capable of enlarging the consensus of inliers, while restraining the consensus of outliers.

Moreover, since our pruning block is feasible to be iteratively performed, we analyze the effect of iteration numbers towards candidate consistency and pose estimation accuracy. As shown in Fig. 8, an increase of inlier ratios is observed after pruning, *i.e.* from 10% to 80%, which indicates the candidates are much more consistent than initial data. The mAP drops after the second iteration, because the number of remained matches is too small to carry out a robust model estimation.

	Annular Conv.	Conv. & Max-pooling
mAP5 (%)	**53.15**	51.25

Table 4. Comparison between the proposed annular convolution and convolution-pooling strategy. "Conv. & Max-pooling" extracts and aggregates local features with convolutions and max-pooling layers, respectively. mAP5 on YFCC100M [34] is listed.

Local Conv.	Global Conv.	Adaptive temp.	mAP5 (%)
✗	✗	✗	45.50
✓	✗	✗	50.38
✓	✓	✗	52.28
✓	✓	✓	53.15

Table 5. Ablation studies of CLNet on individual components, where the models are trained and tested on YFCC100M [35].

Component analysis. We perform ablation studies to shed more light on the rationality of each component in CLNet. Specifically, Table 4 compares the proposed annular convolution and convolution-pooling strategy which has been widely employed in [26, 36]. The annular convolution achieves 1.90% improvements of mAP5 on YFCC100M, demonstrating its effectiveness. Furthermore, we evaluate the necessity of each component by different combinations. As reported in Table 5, the optimal performance cannot be achieved by removing any one of them. The local-to-global consensus learning leads to a 6.78% improvement of mAP5 in total (the third line *v.s.* the first line), and the performance

is further boosted by applying the adaptive temperatures.

5. Conclusion

Given the observed effects of dominant noisy outliers in correspondence selection tasks, we for the first time propose to gradually tailor the putative correspondences into reliable candidates with a local-to-global consensus learning framework. Both local and global graphs are established on-the-fly to *explicitly* describe the consensus in context, leading to better pruning. Our proposed correspondence denoising largely alleviates the randomly distributed outliers in various scenarios, showing significant improvements on multiple benchmarks.

References

[1] Andrea Albarelli, Emanuele Rodolà, and Andrea Torsello. Imposing semi-local geometric constraints for accurate correspondences selection in structure from motion: A game-theoretic perspective. *Int. J. Comput. Vis.*, 97(1):36–53, 2012.

[2] Relja Arandjelovic, Petr Gronat, Akihiko Torii, Tomas Pajdla, and Josef Sivic. Netvlad: Cnn architecture for weakly supervised place recognition. In *IEEE Conf. Comput. Vis. Pattern Recog.*, pages 5297–5307, 2016.

[3] Daniel Barath, Jiri Matas, and Jana Noskova. Magsac: marginalizing sample consensus. In *IEEE Conf. Comput. Vis. Pattern Recog.*, pages 10197–10205, 2019.

[4] Eric Brachmann and Carsten Rother. Neural-guided ransac: Learning where to sample model hypotheses. In *Int. Conf. Comput. Vis.*, pages 4322–4331, 2019.

[5] Matthew Brown and David G Lowe. Automatic panoramic image stitching using invariant features. *Int. J. Comput. Vis.*, 74(1):59–73, 2007.

[6] Ondrej Chum and Jiri Matas. Matching with prosac-progressive sample consensus. In *IEEE Conf. Comput. Vis. Pattern Recog.*, volume 1, pages 220–226. IEEE, 2005.

[7] Ondřej Chum, Jiří Matas, and Josef Kittler. Locally optimized ransac. In *Joint Pattern Recognition Symposium*, pages 236–243. Springer, 2003.

[8] Daniel DeTone, Tomasz Malisiewicz, and Andrew Rabinovich. Superpoint: Self-supervised interest point detection and description. In *IEEE Conf. Comput. Vis. Pattern Recog. Worksh.*, pages 224–236, 2018.

[9] Martin A Fischler and Robert C Bolles. Random sample consensus: a paradigm for model fitting with applications to image analysis and automated cartography. *Communications of the ACM*, 24(6):381–395, 1981.

[10] Yixiao Ge, Haibo Wang, Feng Zhu, Rui Zhao, and Hongsheng Li. Self-supervising fine-grained region similarities for large-scale image localization. In *Eur. Conf. Comput. Vis.*, 2020.

[11] Richard Hartley and Andrew Zisserman. *Multiple view geometry in computer vision*. Cambridge university press, 2003.

[12] Kaiming He, Xiangyu Zhang, Shaoqing Ren, and Jian Sun. Deep residual learning for image recognition. In *IEEE Conf. Comput. Vis. Pattern Recog.*, pages 770–778, 2016.

[13] Sergey Ioffe and Christian Szegedy. Batch normalization: Accelerating deep network training by reducing internal covariate shift. *arXiv preprint arXiv:1502.03167*, 2015.

[14] Yuhe Jin, Dmytro Mishkin, Anastasiia Mishchuk, Jiri Matas, Pascal Fua, Kwang Moo Yi, and Eduard Trulls. Image matching across wide baselines: From paper to practice. *arXiv preprint arXiv:2003.01587*, 2020.

[15] Hyo Jin Kim, Enrique Dunn, and Jan-Michael Frahm. Learned contextual feature reweighting for image geo-localization. In *IEEE Conf. Comput. Vis. Pattern Recog.*, pages 3251–3260. IEEE, 2017.

[16] Thomas N Kipf and Max Welling. Semi-supervised classification with graph convolutional networks. *arXiv preprint arXiv:1609.02907*, 2016.

[17] Alex Krizhevsky, Ilya Sutskever, and Geoffrey E Hinton. Imagenet classification with deep convolutional neural networks. *Communications of the ACM*, 60(6):84–90, 2017.

[18] Charles L Lawson and Richard J Hanson. *Solving least squares problems*. SIAM, 1995.

[19] Liu Liu, Hongdong Li, and Yuchao Dai. Stochastic attraction-repulsion embedding for large scale image localization. In *IEEE Conf. Comput. Vis. Pattern Recog.*, pages 2570–2579, 2019.

[20] David G Lowe. Distinctive image features from scale-invariant keypoints. *Int. J. Comput. Vis.*, 60(2):91–110, 2004.

[21] Jiayi Ma, Ji Zhao, Junjun Jiang, Huabing Zhou, and Xiaojie Guo. Locality preserving matching. *Int. J. Comput. Vis.*, 127(5):512–531, 2019.

[22] Anastasiia Mishchuk, Dmytro Mishkin, Filip Radenovic, and Jiri Matas. Working hard to know your neighbor's margins: Local descriptor learning loss. In *Adv. Neural Inform. Process. Syst.*, pages 4826–4837, 2017.

[23] Kwang Moo Yi, Eduard Trulls, Yuki Ono, Vincent Lepetit, Mathieu Salzmann, and Pascal Fua. Learning to find good correspondences. In *IEEE Conf. Comput. Vis. Pattern Recog.*, pages 2666–2674, 2018.

[24] Raul Mur-Artal, Jose Maria Martinez Montiel, and Juan D Tardos. Orb-slam: a versatile and accurate monocular slam system. *IEEE Transactions on Robotics*, 31(5):1147–1163, 2015.

[25] James Philbin, Michael Isard, Josef Sivic, and Andrew Zisserman. Descriptor learning for efficient retrieval. In *Eur. Conf. Comput. Vis.*, pages 677–691. Springer, 2010.

[26] Charles Ruizhongtai Qi, Li Yi, Hao Su, and Leonidas J Guibas. Pointnet++: Deep hierarchical feature learning on point sets in a metric space. In *Adv. Neural Inform. Process. Syst.*, pages 5099–5108, 2017.

[27] Rahul Raguram, Ondrej Chum, Marc Pollefeys, Jiri Matas, and Jan-Michael Frahm. Usac: a universal framework for random sample consensus. *IEEE Trans. Pattern Anal. Mach. Intell.*, 35(8):2022–2038, 2012.

[28] Shaoqing Ren, Kaiming He, Ross Girshick, and Jian Sun. Faster r-cnn: Towards real-time object detection with region proposal networks. In *Adv. Neural Inform. Process. Syst.*, pages 91–99, 2015.

[29] Ethan Rublee, Vincent Rabaud, Kurt Konolige, and Gary Bradski. Orb: An efficient alternative to sift or surf. In *Int. Conf. Comput. Vis.*, pages 2564–2571. Ieee, 2011.

[30] Paul-Edouard Sarlin, Daniel DeTone, Tomasz Malisiewicz, and Andrew Rabinovich. Superglue: Learning feature matching with graph neural networks. In *IEEE Conf. Comput. Vis. Pattern Recog.*, pages 4938–4947, 2020.

[31] Noah Snavely, Steven M Seitz, and Richard Szeliski. Modeling the world from internet photo collections. *Int. J. Comput. Vis.*, 80(2):189–210, 2008.

[32] Weiwei Sun, Wei Jiang, Eduard Trulls, Andrea Tagliasacchi, and Kwang Moo Yi. Acne: Attentive context normalization for robust permutation-equivariant learning. In *IEEE Conf. Comput. Vis. Pattern Recog.*, pages 11286–11295, 2020.

[33] Richard Szeliski. Image mosaicing for tele-reality applications. In *Proceedings of 1994 IEEE Workshop on Applications of Computer Vision*, pages 44–53. IEEE, 1994.

[34] Bart Thomee, David A Shamma, Gerald Friedland, Benjamin Elizalde, Karl Ni, Douglas Poland, Damian Borth, and Li-Jia Li. Yfcc100m: The new data in multimedia research. *Communications of the ACM*, 59(2):64–73, 2016.

[35] Akihiko Torii, Relja Arandjelovic, Josef Sivic, Masatoshi Okutomi, and Tomas Pajdla. 24/7 place recognition by view synthesis. In *IEEE Conf. Comput. Vis. Pattern Recog.*, pages 1808–1817, 2015.

[36] Yue Wang, Yongbin Sun, Ziwei Liu, Sanjay E Sarma, Michael M Bronstein, and Justin M Solomon. Dynamic graph cnn for learning on point clouds. *ACM Trans. Graph.*, 38(5):1–12, 2019.

[37] Jianxiong Xiao, Andrew Owens, and Antonio Torralba. Sun3d: A database of big spaces reconstructed using sfm and object labels. In *IEEE Conf. Comput. Vis. Pattern Recog.*, pages 1625–1632, 2013.

[38] Jiahui Zhang, Dawei Sun, Zixin Luo, Anbang Yao, Lei Zhou, Tianwei Shen, Yurong Chen, Long Quan, and Hongen Liao. Learning two-view correspondences and geometry using order-aware network. In *Int. Conf. Comput. Vis.*, pages 5845–5854, 2019.

[39] Chen Zhao, Zhiguo Cao, Chi Li, Xin Li, and Jiaqi Yang. Nm-net: Mining reliable neighbors for robust feature correspondences. In *IEEE Conf. Comput. Vis. Pattern Recog.*, pages 215–224, 2019.

[40] Chen Zhao, Zhiguo Cao, Jiaqi Yang, Ke Xian, and Xin Li. Image feature correspondence selection: A comparative study and a new contribution. *IEEE Trans. Image Process.*, 29:3506–3519, 2020.

A. Appendix

A.1. Comparison with NGRANSAC [4]

	Outdoor (%)		
	mAP5	mAP10	mAP20
NGRANSAC [4]	49	54	59
Our CLNet	**54**	**60**	**66**
	Indoor (%)		
	mAP5	mAP10	mAP20
NGRANSAC [4]	**14**	20	29
Our CLNet	**14**	**21**	**31**

Table 6. Comparison with NGRANSAC on wide-baseline image matching. mAPs (%) of recovered camera poses are reported.

NGRANSAC [4] aims at correspondence selection, but on a different benchmark. So we do not include their results in Table 1 of the main paper, instead, we fairly compare with them by training our CLNet on the same benchmark as that used in NGRANSAC. Specifically, one sequence from YFCC100M [34] and one sequence from SUN3D [37] are selected for jointly training. Five sequences from YFCC100M are employed for testing the outdoor scenarios, and sixteen sequences from SUN3D are used for testing the indoor scenarios. We adopt all the same experimental settings as [4]. NGRANSAC uses PointCN [23] to guide model hypothesis search, which utilizes the strength of both PointCN and RANSAC. For a fair comparison, we also employ RANSAC [9] as a post-processing of our CLNet. The results are shown in Table 6. Compared with NGRANSAC, our CLNet achieves significantly superior results on outdoor sequences, *i.e.* at least 5% improvement in terms of mAPs. Better performance on indoor sequences are also observed.

A.2. Analysis on k for Local Graphs

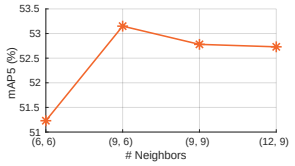

Figure 9. The effect of different numbers (k) of neighbors in local graphs. $(\cdot, \cdot)$ denote the k values in local graphs of the first and the second pruning blocks, respectively. Results without RANSAC [9] on YFCC100M [34] are reported in terms of mAP5.

We adopt local consensus learning in the proposed pruning blocks, where local graphs are established by k-nearest neighbor search. Specifically, two pruning blocks are utilized sequentially in our framework. We select $k = 9$ in the first block and $k = 6$ in the second block. Note we suggest using a smaller k in the second pruning block, since $N/2$ correspondences are consumed in this block.

To verify the effectiveness of such a design, we conduct experiments by using different combinations of values of k. As illustrated in Fig. 9, our CLNet achieves the optimal performance with a combination of $(9, 6)$. The results with other combinations still outperforms state-of-the-art methods [32, 38] (Please refer to Table 1 of the main paper for results of competitors).

A.3. Visualizations

Visual results on YFCC100M and SUN3D are shown in this section. We illustrate the selected correspondences by state-of-the-art methods [23, 32] and our CLNet in Fig. 10 and Fig. 11. We use red and green lines to distinguish the false positives (outliers) and true positives (inliers) identified by the ground-truth ("GT"). Note that the ground-truth labels are generated by the epipolar constraint [11], which are inevitably noisy, *i.e.* outliers might be falsely classified into inliers. For our CLNet, we show the matches selected from the denoised candidates, since the parametric model is estimated from the selected results. The results with RANSAC as a post-processing are also illustrated. Compared with the competitors, the preserved matches of our CLNet are much more consistent with fewer outliers on both YFCC100M and SUN3D datasets.

In order to discuss the limitations of our method, we show some failure cases of our CLNet. As illustrated in Fig. 12, outliers dominate the denoised candidates. One can observe that ground-truth labels are remarkably unreliable in these cases, where the keypoints of many inliers are actually located in visually inconsistent regions. The unreliable ground-truth labels may mislead the consensus learning in our method. We attempt to mitigate such an effect by introducing an adaptive temperature in the binary cross-entropy loss (see Eq. (9)&(11) of the main paper), which has been proven effective in ablation studies (Table 5 of the main paper). We expect to further improve the robustness of our method towards noisy ground-truth labels in future works.

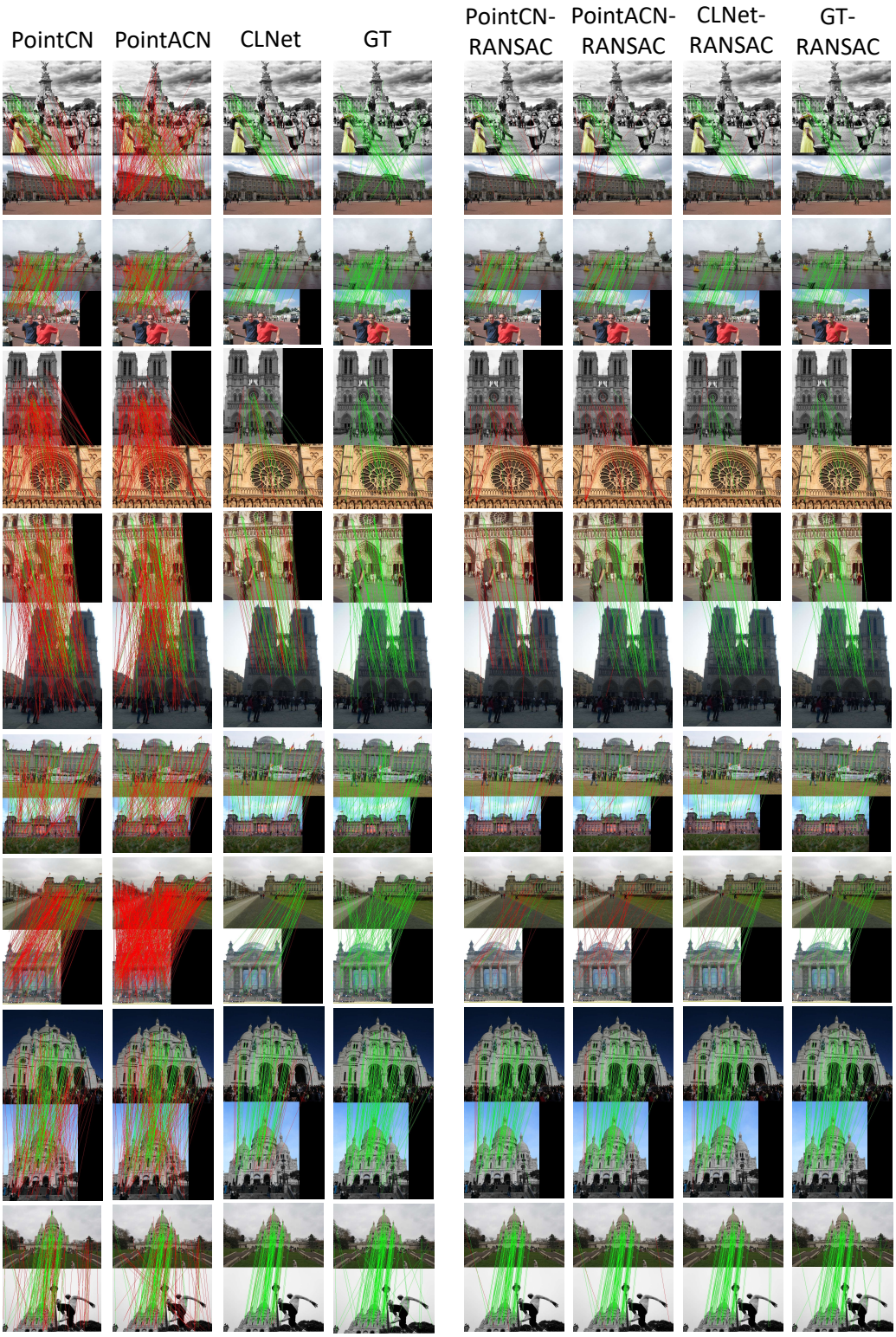

Figure 10. Visualizations on YFCC100M [34]. "GT" denotes the ground-truth. The illustrated correspondences are selected by the evaluated methods, where green and red lines indicate true positives (inliers) and false positives (outliers), respectively. For our CLNet, the matches selected from the denoised candidates are shown, since they are used for the model estimation. "$*$-RANSAC" represents using RANSAC as a post-processing.

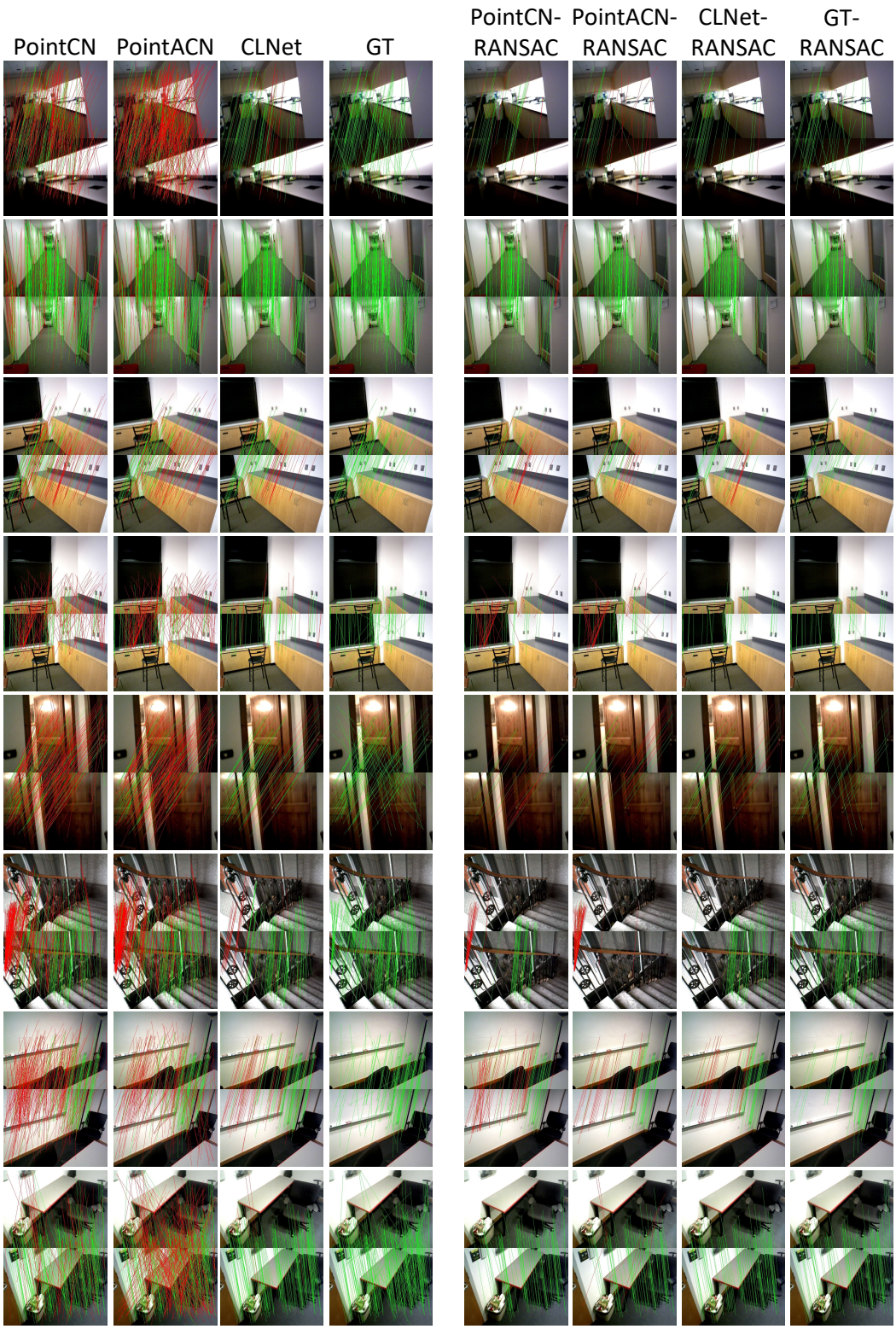

Figure 11. Visualizations on SUN3D [37]. "GT" denotes the ground-truth. The illustrated correspondences are selected by the evaluated methods, where green and red lines indicate true positives (inliers) and false positives (outliers), respectively. For our CLNet, the matches selected from the denoised candidates are shown, since they are used for the model estimation. "$*$-RANSAC" represents using RANSAC as a post-processing.

Figure 12. Failure cases of our CLNet on YFCC100M [34] and SUN3D [37].